Figures of merit for microwave photonic phase shifters based on semiconductor optical amplifiers

Juan Sancho,[*] **Juan Lloret, Ivana Gasulla, Salvador Sales, and José Capmany**

ITEAM Research Institute, Optical and Quantum Communications Group, Universidad Politécnica de Valencia, Camino de Vera s/n, 46022 Valencia, Spain

[*]*juasandu@upvnet.upv.es*

Abstract: We theoretically and experimentally compare the performance of two fully tunable phase shifter structures based on semiconductor optical amplifiers (SOA) by means of several figures of merit common to microwave photonic systems. A single SOA stage followed by a tailored notch filter is compared with a cascaded implementation comprising three SOA-based phase shifter stages. Attention is focused on the assessment of the RF net gain, noise figure and nonlinear distortion. Recommendations on the performance optimization of this sort of approaches are detailed.

References and links

1. J. Capmany and D. Novak, "Microwave photonics combines two worlds," Nat. Photonics **1**(6), 319–330 (2007).
2. J. Yao, "Microwave photonics," J. Lightwave Technol. **27**(3), 314–335 (2009).
3. J. Capmany, B. Ortega, and D. Pastor, "A tutorial on microwave photonic filters," J. Lightwave Technol. **24**(1), 201–229 (2006).
4. D. Dolfi, P. Joffre, J. Antoine, J.-P. Huignard, D. Philippet, and P. Granger, "Experimental demonstration of a phased-array antenna optically controlled with phase and time delays," Appl. Opt. **35**(26), 5293–5300 (1996).
5. R. W. Boyd and D. J. Gauthier, "Slow and fast light," Prog. Opt. **43**, 497–530 (2002).
6. S. Sales, W. Xue, J. Mork, and I. Gasulla, "Slow and fast light effects and their applications to microwave photonics using semiconductor optical amplifiers," J. Lightwave Technol. **58**, 3022–3038 (2010).
7. J. Lloret, J. Sancho, M. Pu, I. Gasulla, K. Yvind, S. Sales, and J. Capmany, "Tunable complex-valued multi-tap microwave photonic filter based on single silicon-on-insulator microring resonator," Opt. Express **19**(13), 12402–12407 (2011).
8. J. Sancho, S. Chin, M. Sagues, A. Loayssa, J. Lloret, I. Gasulla, S. Sales, L. Thevenaz, and J. Capmany, "Dynamic microwave photonic filter using separate carrier tuning based on stimulated brillouin scattering in fibers," IEEE Photon. Tech. Lett. **22**(23), 1753–1755 (2010).
9. J. Mørk, R. Kjær, M. van der Poel, and K. Yvind, "Slow light in a semiconductor waveguide at gigahertz frequencies," Opt. Express **13**(20), 8136–8145 (2005).
10. W. Xue, Y. Chen, F. Öhman, S. Sales, and J. Mørk, "Enhancing light slow-down in semiconductor optical amplifiers by optical filtering," Opt. Lett. **33**(10), 1084–1086 (2008).
11. W. Xue, S. Sales, J. Capmany, and J. Mørk, "Wideband 360 ° microwave photonic phase shifter based on slow light in semiconductor optical amplifiers," Opt. Express **18**(6), 6156–6163 (2010).
12. J. Sancho, J. Lloret, I. Gasulla, S. Sales, and J. Capmany, "Fully tunable 360° microwave photonic phase shifter based on a single semiconductor optical amplifier," Opt. Express **19**(18), 17421–17426 (2011).
13. C. Cox, *Analog optical links* (U.K. Cambridge Univ. Press, 2004)
14. S. Ó. Dúill, E. Shumakher, and G. Eisentein, "Noise properties of microwave phase shifters based on semiconductor optical amplifiers," J. Lightwave Technol. **28**(5), 791–797 (2010).
15. J. Lloret, F. Ramos, W. Xue, J. Sancho, I. Gasulla, S. Sales, J. Mork, and J. Capmany, "The influence of optical filtering on the noise performance of microwave photonic phase shifters based on SOAs," J. Lightwave Technol. **29**(12), 1746–1752 (2011).
16. I. Gasulla, J. Sancho, J. Capmany, J. Lloret, and S. Sales, "Intermodulation and harmonic distortion in slow light Microwave Photonic phase shifters based on Coherent Population Oscillations in SOAs," Opt. Express **18**(25), 25677–25692 (2010).

1. Introduction

The interaction field between microwave and optical signals is known as microwave photonics (MWP) [1], an emergent area of research which enables the generation, transport and processing of radio frequency (RF), microwave and millimeter-wave signals directly in the optical domain [2]. Some of the most exciting motivations behind the MWP field are attributed to its potential application to implement wideband reconfigurable filters [3], optoelectronic oscillators [2] and optically fed phased array antennas [4]. To this end, the efficient design of broadband tunable microwave phase shifters and true time delay lines is of key importance. For this purpose, the exploitation of Slow and Fast Light (SFL) effects, which refers to the ability of controlling the group velocity of light in a certain media, has arisen as a very promising alternative in the past ten years [5]. To date, several approaches spanning different technology platforms have already been demonstrated for the implementation of microwave phase shifting tasks [6–8].

One of the most successful approaches reported so far is based on the so-called coherent population oscillations (CPO) in semiconductor optical amplifiers (SOA) [6], since it may provide a realistic solution providing on-chip integration at high operation frequencies among others. CPO effect is responsible for gain and refractive index dynamics in SOAs, giving as a result a phase shift of the modulating microwave signal [9]. The RF phase slow-down experienced by an RF signal after propagating through an SOA can be greatly enhanced by optical filtering the long wavelength modulation sideband prior to detection (~150° at 19 GHz), since the refractive index dynamics is more efficiently exploited [10]. Besides, phase shifts up to 360° over a 40 GHz bandwidth have been recently reached when cascading several SOA based stages [11]. This technique can provide a nearly linear phase transition higher than 360° with ~10 dB of power variation along the entire tunability range. However, the previously reported work resorts to the use of optical notch filters solely to reject the low frequency sideband aiming at increasing the microwave phase shift. In this way, a conveniently designed notch filter has been proposed [12] in order to obtain the proper phase and power attenuation combination after propagating through a single SOA and thus, achieving a fully tunable 360° microwave phase shifter provided by both fast and slow light effects. This means reducing four SOAs and two optical filters in comparison with the previously reported approach [11].

From the microwave link point of view, several figures of merit (FOM) must be employed to evaluate these phase shifter implementations to report objective data regarding the degradation of the system performance [13]. Different issues related to the characterization of SFL SOA-based elements have been addressed so far, including those concerning the noise degradation [14–15] and nonlinear distortion leading to the generation of harmonic and intermodulation components [16]. In this paper, the performance of MWP phase shifters based on a single SOA followed by a tailored notch filter and a cascaded implementation comprising three SOA-based phase shifter stages are theoretically and experimentally evaluated in terms of several FOMs. In particular, gain, noise and nonlinear distortion are characterized as a function of the phase tunability control mechanism. Attending to the results, recommendations on the optimization of this sort of structures are also reported.

2. Experimental setup

The experimental layout of an SOA-based fully tunable MWP phase shifter is illustrated in Fig. 1. A distributed-feedback laser diode (DFB-LD) was used as a light source. Two RF signals with frequencies f1 = 20 GHz and f2 = 20.5 GHz were imprinted on the optical carrier by means of a zero-chirp electro-optic modulator (EOM). At the erbium doped fiber amplifier (EDFA) output, a variable optical attenuator (VOA) is used to assure the proper optical power at the phase shifter input. The phase shifter was comprised of either a single photonic shifting stage (PSS) or cascaded PSSs. The single PSS approach was made up by an SOA followed by a tailored fiber Bragg grating (FBG) [12], as Fig. 1(a) illustrates, while the cascaded structure was formed by three consecutive PSSs [11], as shown in Fig. 1(b). The use of regeneration

stages (RS) in-between individual PSS was requested in order to restore the modulation sideband suppressed by previous filtering [11]. The tailored FBG spectral response can be found in [12], while the magnitude and phase response of the three identical FBGs used for the cascaded structure can be found in [16]. The phase shifter output was detected and finally measured by using an electrical spectrum analyzer (ESA).
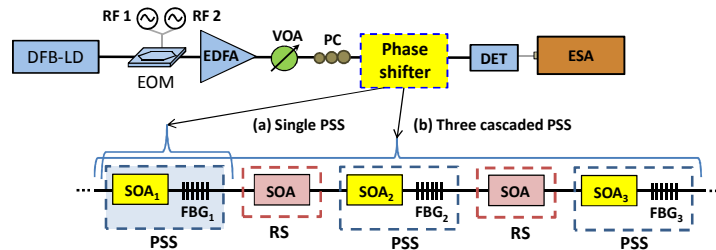

Fig. 1. Experimental setup of the MWP phase shifter based on SOAs. (a) SOA + tailored FBG based performance and (b) cascaded implementation.

3. Figures of merit results

The performance of both phase shifting approaches must be evaluated in terms of several FOMs due to the active and nonlinear nature of the SOA device [6]. Special attention must be paid on the fact that in photonic microwave links, additional noise can degrade the noise figure (NF) [14–15]. Furthermore, the nonlinearity of the external modulator and in the optical processing stage can increase the nonlinear distortion [16].

The most common metrics used are the RF net power gain, the noise figure and the spurious free dynamic range (SFDR) involving 2nd and 3rd order intermodulation products [13]. These metrics have been evaluated as a function of the PSS injection currents. Experimental results have been theoretically validated by comparing with the theoretical expressions for the figures of merits provided in section IV of [6].

3.1 Noise figure

In order to evaluate the signal degradation in MWP links related to the system added noise sources, the NF is the most frequently used metric. The NF is defined as the ratio of the signal-to-noise ratio at the input, SNR_{in}, to the signal-to-noise ratio at the output, SNR_{out} [6]. Besides, the SNR can be defined as the ratio between the RF power and the noise power level [6]. Several noise sources contribute to the total output noise level. In particular, the relative intensity noise (RIN) of the DFB-LD, the phase noise of the RF synthesizer, the amplified emission noise generated by the EDFA and all the five SOAs and the thermal and shot noises added by the detector. Under typical realistic conditions, the dominating term contribution to the total output noise level is due to the signal-spontaneous beat-note at the SOA output [14].

Figure 2(a) illustrates the RF power levels for the signal and noise floor as a function of the injection current when the SOA is fed by two different optical powers. The system bandwidth for noise integration purposes was 100 MHz. Noise degradation by more than 10 dB is observed. On the other hand, the evolution of the output SNR and NF is shown in Fig. 2(b). An average output SNR_{out} level ~32 dB is reached, while 48 dB of SNR_{in} is obtained at the phase shifter input. On the right, peaks in the NF response match the depth dips in the SNR_{out} curve. NF upper limit of 36 dB is reached, while its average level turns ~15 dB.

Figure 3(a) depicts the RF power levels for the signal and noise floor at the input and output of the cascaded implementation, while both the output SNR and NF are illustrated in Fig. 3(b). An interesting noise behavior can be observed in Fig. 3(a), since its power level keeps constant for the two initial PSSs while, by increasing the injection current into the third PSS, the noise level increases accordingly. The RSs were working under deep saturation regime, therefore the noise floor became equalized at their output. An output SNR experiencing three smooth notches is obtained, as observed in Fig. 3(b). In average, the SNR

level centers at 18 dB, which means a 14 dB degradation regarding the implementation based on a single PSS. A minimum SNR level of 9 dB is obtained, which corresponds to the maximum value of the NF. Yet, this maximum level rises up to 37 dB, while getting an average value of around 30 dB. This means an increase of the NF level of ~15 dB with respect to the case in which a single PSS based phase shifter is realized.

It is well-known that the added noise in semiconductor waveguides is proportional to its power gain [15]. By increasing the input optical power and reducing the injection current, the power gain can be lowered without altering the CPO efficiency while operating the SOA in the saturation regime [9]. As a consequence, the noise floor could be lowered and the SNR_{out} increased, giving as a result a NF reduction. Besides, for the cascaded implementation, the total noise at the system output can be reduced by band-pass filtering each PSS output. In such a way, part of the added noise at the stage output will not be amplified by the following cascades stages. In addition, optical filtering prior to photodetection will also lower the noise level and, in consequence, the NF.
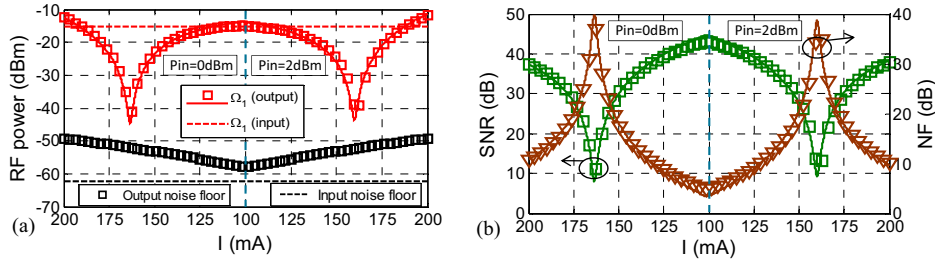

Fig. 2. Theoretical (solid lines) and experimental (markers and dashed lines) RF power and noise level at the (a) input (dashed lines) and output (markers), (b) output SNR and NF as a function of the SOA injection currents when the input power is fixed at 0dBm or 2dBm.
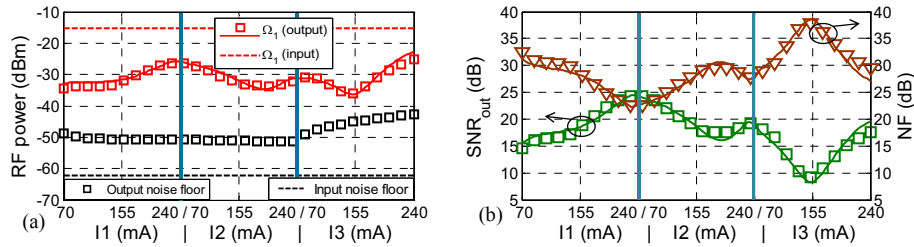

Fig. 3. Theoretical (solid lines) and experimental (markers and dashed lines) RF power and noise level at the (a) input (dashed lines) and output (markers), (b) output SNR and NF as a function of the injection currents into the three PSS.

3.2 Net RF Power gain

The RF net power gain of a MWP link can be defined as the ratio between the RF power delivered at the detector output and the available RF power at the modulation device input [6].

Figures 4(a) and 4(b) resort for the RF net gain as a function of a single and three cascaded PSSs injection currents, respectively. RF power levels obtained at the phase shifter input and each PSS output have been used to accomplish all the gain curves. Results in Fig. 4(a) have been represented for two different optical input powers. As expected, the same behavior of the RF power for the fundamental tone illustrated in Figs. 2(a) and 3(a) is observed. More than 25 dB of gain variation is achieved in Fig. 4(a) by tuning the injection current. However, around 10 dB is obtained at the output of the third PSS. Besides, an average RF gain level of ~-5 dBm is obtained for a single SOA, while the three cascaded PSSs based approach accomplishes −17 dBm. This means gain degradation in ~12 dB.

The observed low RF net gain values at the output of the three PSSs are mainly due to saturation effects in all the SOAs and sideband suppression due to the FBG. However, it can be readily improved by using amplification before detection. Yet, the RF power variation, especially for the single PSS approach, represents a serious constraint which could limit its assembling in real applications. It is determined by the underlying physics of the CPO phenomenon accompanied by the optical filtering. The phase shift transitions abruptness depends on the saturation status of all the SOAs and the degree of filtering of the lower frequency modulation sideband [10]. By adjusting the polarization state of the optical signal at each SOA input, the CPO efficiency can be controlled. This way less deep RF power dips and consequently more relaxed linear behavior of the phase shift can be achieved. As suspected, this fact would reduce also the total NF variation.
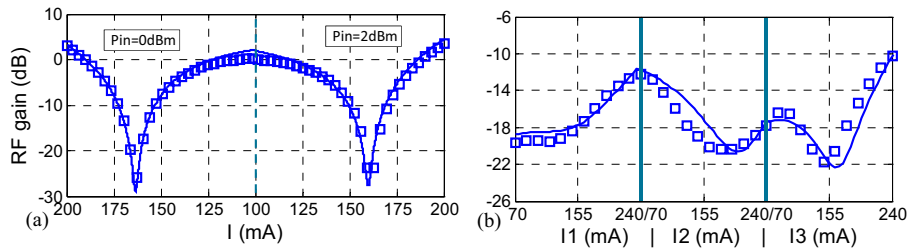

Fig. 4. Theoretical (solid lines) and experimental (markers) RF net gain as a function of (a) one and (b) three PSS injection currents.

3.3 SFDR

The spurious-free dynamic range (SFDR) is the most common metric used for evaluating the nonlinear behavior of a MWP link. Two-tone SFDR is defined as the carrier-to-noise ratio when the noise floor contained in 1-Hz bandwidth equals to the power of a given order intermodulation product [6]. Depending on the reference signal, $SFDR_2$ and $SFDR_3$ are defined. In particular, $SFDR_2$ and $SFDR_3$ refer to the 2nd and 3rd order distortion respectively. To obtain these values, the difference between the power intersection points with the noise curve relative to the fundamental (Ω_1 and Ω_2), and the 2nd ($\Omega_2 - \Omega_1$, $\Omega_2 + \Omega_1$) or 3rd ($2\Omega_1 - \Omega_2$ and $2\Omega_2 - \Omega_1$) order harmonics has been calculated.

On one hand, photodetected RF power versus the RF input power to the EOM results are represented in Figs. 5(a) and 6(a) for every signal order, harmonic and intermodulation products of interest. Dashed lines correspond to the RF power at the phase shifter input. These SFDR values from each pair of both 2nd and 3rd intermodulation products reach 83 dB·Hz$^{1/2}$ and 100 dB·Hz$^{2/3}$ respectively. At the single PSS output, $SFDR_2$ and $SFDR_3$ values around 67 dB·Hz$^{1/2}$ and 93 dB·Hz$^{2/3}$ are achieved. While around 45 dB·Hz$^{1/2}$ and 62 dB·Hz$^{1/2}$ $SFDR_2$, and 75 dB·Hz$^{2/3}$ $SFDR_3$ values are obtained at the third PSS output. The low power behavior, experienced by the $\Omega_2 - \Omega_1$ term at the third PSS output, relies on the nonlinear behavior of the low-band frequency filter used by the VNA.

On the other hand, Figs. 5(b) and 6(b) illustrate the evolution for both the $SFDR_2$ and $SFDR_3$ as a function of a single and three cascaded PSS injection currents respectively. Results in Fig. 5(b) have been represented for two different optical powers at the SOA input. It is clearly observed that the tendency is roughly the same for the $SFDR_2$ and $SFDR_3$ terms. At the single PSS output, average $SFDR_2$ and $SFDR_3$ values around 63 dB·Hz$^{1/2}$ and 88 dB·Hz$^{2/3}$ are achieved. While at the third PSS output, average values around 45 dB·Hz$^{1/2}$ and 50 dB·Hz$^{1/2}$ $SFDR_2$ and 93 dB·Hz$^{2/3}$ $SFDR_3$ are obtained. This implies an SFDR difference of ~14 dB and ~20 dB for the second and third order distortion respectively comparing both

phase shifting structures. The dip deviations in their responses indicates that the SFDR dynamics do not follow the same behavior as a function of the injection current as compared with that observed either in Fig. 2(a) or 3(a). This can be understood regarding 2nd and 3rd order distortion, since their RF powers are slightly deviated as a function of the bias point.

In terms of the nonlinear distortion optimization, the limiting factor relies on the dependence of the generation efficiency of the 2nd and 3rd order products on the bias currents. The minimum values of SFDR could be further improved by engineering the SOAs in order to minimize the above-mentioned dependence.
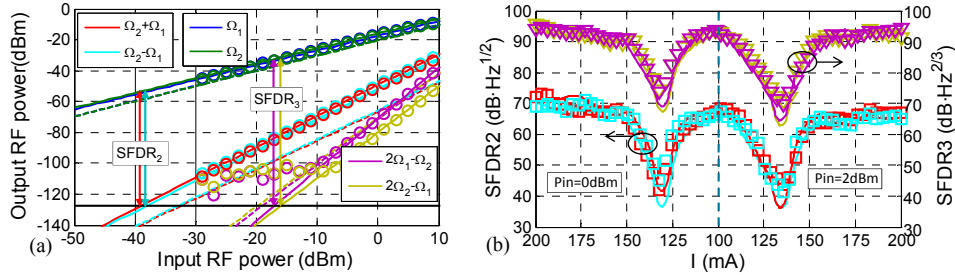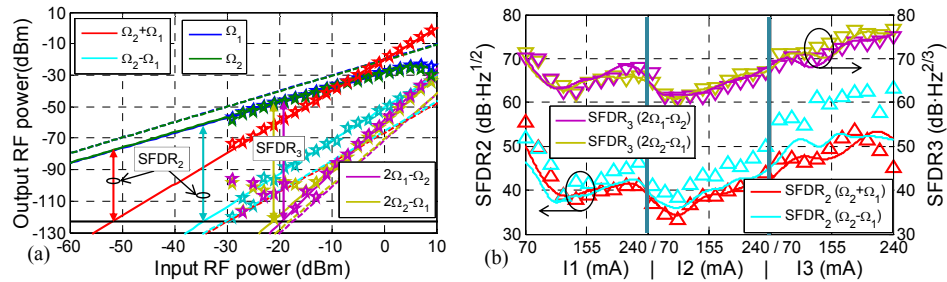

Fig. 5. (a) Theoretical (lines) and experimental (markers) RF power from the fundamental, IMD$_2$ and IMD$_3$ terms vs. input RF power at the third PSS output when I = 200 mA. (b) SFDR2 and SFDR3 as a function of the PSS injection current.

Fig. 6. (a) Theoretical (lines) and experimental (markers) RF power from the fundamental, IMD$_2$ and IMD$_3$ terms vs. input RF power at the third PSS output when $I_{PSS1} = I_{PSS2} = I_{PSS3} = 240$ mA. (b) SFDR2 and SFDR3 as a function of the three PSS injection currents.

3. Conclusions

In summary, the performance of two MWP phase shifter implementations has been evaluated and compared in terms of several figures of merit. In particular, the evaluation has focused on the assessment of the RF net gain, NF and SFDR as a function of the bias currents injected into the PSSs, which act as the phase shifting control mechanism. The behavior of the net gain and NF is mainly determined by the RF output power, since the SFDR is at last imposed by the slightly changes in the slope of the generated distortion as function of the bias currents. Maximum RF net gain variation of 27 dB, upper NF limit of 36 dB and minimum SFDR$_3$ of 70 dB·Hz$^{2/3}$ have been obtained for a single PSS, while the cascaded structure has reached ~10 dB gain variation, 37 dB maximum NF and 60 dB·Hz$^{2/3}$ minimum SFDR$_3$. On the other hand, the average levels at the output of the cascaded structure turn in a system degradation of 12 dB, 15 dB and 20 dB for the RF net gain, NF and SFDR respectively compared with the single PSS based approach. Optimized performance can be accomplished, especially for the cascaded structure, by proper adjustment of the optical input power and the bias currents injected into all the SOAs. Besides, the polarization control plays an important role at the time of dealing with phase shifting linearization purposes. Nonetheless, sharp phase slopes, and therefore deeper power dips, are required to reach the desired 360° in the phase shifter based

on a single PSS. This way the system performance becomes diminished in terms of gain, noise and SFDR due to the output power dependence. For less phase shift requirements, i.e. less than 2π, different filtering scenarios can be considered in order to reduce the dip depth. However, this implementation can be efficiently employed to obtain discrete phase shifts, i.e. π, without power penalties, high bandwidth and very fast tunability speed.

Acknowledgments